OAK RIDGE NATIONAL LABORATORY LIBRARY

3 4456 0003198 0

ORNL/TM-9688

ornl

OAK RIDGE NATIONAL LABORATORY

MARTIN MARIETTA

Effects of an Alpha Particle Slowing-Down Distribution on Tokamak Ballooning Modes

D. A. Spong
D. E. Hastings
D. J. Sigmar
W. A. Cooper

OAK RIDGE NATIONAL LABORATORY
CENTRAL RESEARCH LIBRARY
CIRCULATION SECTION
4500N ROOM 175
LIBRARY LOAN COPY
DO NOT TRANSFER TO ANOTHER PERSON
If you wish someone else to see this report, send in name with report and the library will arrange a loan.

OPERATED BY
MARTIN MARIETTA ENERGY SYSTEMS, INC.
FOR THE UNITED STATES
DEPARTMENT OF ENERGY

Printed in the United States of America. Available from
National Technical Information Service
U.S. Department of Commerce
5285 Port Royal Road, Springfield, Virginia 22161
NTIS price codes—Printed Copy: A03; Microfiche A01

This report was prepared as an account of work sponsored by an agency of the United States Government. Neither the United States Government nor any agency thereof, nor any of their employees, makes any warranty, express or implied, or assumes any legal liability or responsibility for the accuracy, completeness, or usefulness of any information, apparatus, product, or process disclosed, or represents that its use would not infringe privately owned rights. Reference herein to any specific commercial product, process, or service by trade name, trademark, manufacturer, or otherwise, does not necessarily constitute or imply its endorsement, recommendation, or favoring by the United States Government or any agency thereof. The views and opinions of authors expressed herein do not necessarily state or reflect those of the United States Government or any agency thereof.

ORNL/TM-9688
Dist. Category UC-20g

Fusion Energy Division

EFFECTS OF AN ALPHA PARTICLE SLOWING-DOWN DISTRIBUTION ON TOKAMAK BALLOONING MODES

D. A. Spong
D. E. Hastings
D. J. Sigmar
W. A. Cooper

Date Published - December 1985

OAK RIDGE NATIONAL LABORATORY LIBRARY
3 4456 0003198 0

Prepared by
OAK RIDGE NATIONAL LABORATORY
Oak Ridge, Tennessee 37831
operated by
MARTIN MARIETTA ENERGY SYSTEMS, INC.
for the
U.S. DEPARTMENT OF ENERGY
under Contract No. DE-AC05-84OR21400

CONTENTS

ABSTRACT..... v

I. INTRODUCTION..... 1

II. BASIC EQUATIONS..... 2

III. DISCUSSION OF RESULTS..... 6

IV. CONCLUSIONS..... 18

REFERENCES..... 20

APPENDIX A: EVALUATION OF THE $H(\eta,\delta)$ INTEGRAL..... 21

ABSTRACT

Energetic trapped alpha particles interact through their precessional drift with high-mode-number ballooning modes in tokamaks. Due to the energy dependence of the precessional drift, the consequences of this interaction depend on the form of the alpha distribution function. Results are compared here for two forms of alpha distribution: a Maxwellian and a slowing-down distribution. The latter has a significantly greater influence on ballooning stability because of the larger fraction of particles in the energy range of the drift resonance. Also, due to the dependence on the critical velocity ($\propto T_e^{1/2}$), the stability boundaries and growth rates now are strong functions of the background electron temperature T_e. Parameters typical of tokamak breakeven experiments such as the Tokamak Fusion Test Reactor (TFTR) [Phys. Rev. Lett. 52, 1492 (1984)] are considered.

I. INTRODUCTION

Recently, there has been significant interest in the effect of hot particle populations[1-6] on ballooning modes in tokamaks. It has become clear that in the low-frequency limit (where the kinetic ballooning mode frequency ω is much smaller than the hot particle precessional drift ω_{dH}) a hot component can stabilize ballooning modes,[3] while in the higher-frequency range ($\omega \lesssim \omega_{dH}$) the hot component is destabilizing. For the case of alpha particles, a detailed analysis of these effects[5] has indicated that over typical parameter regimes of reacting plasmas, the alpha collisional coupling to the background plasma is such that $\omega \lesssim \omega_{dH}$. Including the fact that the alpha pressure gradient in the central region is expected to be a sizable fraction (one-third to one-half) of the plasma pressure gradient has yielded substantial deterioration in the ballooning stability boundaries for large-aspect-ratio, circular tokamaks.

This previous analysis,[5] however, was based on a Maxwellian energy distribution model to simplify the resulting resonant velocity-space integrals and to model quasi-thermalized alphas. The hot species temperature was then varied over the energy ranges of the slowing-down alpha particles. In this paper, we consider the exact slowing-down distribution [i.e., $f_H \sim (v^3 + v_c^3)^{-1}$] and compare results obtained using it with those obtained from a Maxwellian having the same energy and density moments. Both distributions also contain a very peaked (about $v_{\|}/v = 0$) distribution in pitch angle in accordance with a deeply trapped ordering, as was employed in Ref. 5.

II. BASIC EQUATIONS

The ballooning equations solved here are based on the two coupled integro-differential equations developed in Ref. 1 from the gyrokinetic formalism. The two hot species distributions we consider are:

$$f_{Max} = a_1 N_H \exp(-E/T_H)\exp(-b_0\hat{\kappa}^2) \ , \tag{1}$$

where

$$\hat{\kappa}^2 = \frac{1}{2\varepsilon}\left(\frac{E}{\mu B_0} - 1 + \varepsilon\right) \ ,$$

ε = inverse aspect ratio ,

B_0 = magnetic field at $\Theta = 0$,

a_1 = normalization factor chosen so that

$$\int \frac{d\Theta}{2\pi} \int F_H \, d^3v = N_H(r) \ ,$$

and

$$f_{s.d.} = \begin{cases} \dfrac{a_2 N_H(r)}{v^3 + v_c^3} \exp(-b_0\hat{\kappa}^2) \ , & \dfrac{M_H v^2}{2} < 3.5 \text{ MeV} \\ 0 \ , & \dfrac{M_H v^2}{2} > 3.5 \text{ MeV} \end{cases} \ , \tag{2}$$

where

$$v_c^3 = 3\sqrt{\pi}\,\frac{M_e}{M_H}\,[Z]\left(\frac{2T_e}{M_e}\right)^{3/2} ,$$

$$[Z] = \sum_{\text{ions}} \frac{Z_i^2 n_i/A_i}{n_e} ,$$

A_i = atomic mass number ,

Z_i = charge (in units of proton charge) ,

n_e, T_e, M_e = background plasma electron density, temperature, and mass,

a_2 = normalization factor chosen so that

$$\int \frac{d\Theta}{2\pi} \int F_H \, d^3v = N_H(r) .$$

The ballooning equation derived in the case of the Maxwellian distribution, given in Ref. 5, is

$$\frac{d}{d\Theta}(1 + h^2)\,\frac{d\tilde{\phi}}{d\Theta} + \left\{\Omega\left(\Omega - \frac{\omega_p}{\omega_A}\right)\left(1 + h^2\right) + \left(\cos\Theta + h\sin\Theta\right) \times \left[\alpha_c + \frac{3}{4}\,\alpha_H G(\Theta)\right]\right\}\tilde{\phi}$$

$$= \frac{\alpha_H}{2}\,\frac{(\cos\Theta + h\sin\Theta)G(\Theta)H(\eta)\tilde{\phi}(\Theta = 2m\pi)}{1 - \frac{1}{2q^2}\left\{\alpha_c + \frac{3}{2}\,\alpha_H G(0)\left[1 - \frac{2}{3}\,H(\eta)\right]\right\}} \tag{3}$$

[for $2(m - 1)\pi \leq \Theta \leq 2(m + 1)\pi$],

where

$$\Omega = \frac{\omega}{\omega_A} , \qquad \omega_A = \frac{v_A}{qR} ,$$

$$s = \frac{rq'}{q} , \qquad \alpha_c = -\frac{Rq^2 p_c'}{B^2/8\pi} , \qquad \alpha_H = -\frac{Rq^2 T_H n_H'}{B^2/8\pi} ,$$

$$H(\eta) = \frac{2}{\sqrt{\pi}} \int_0^\infty \frac{x^{5/2} e^{-x}\, dx}{x - \eta} = \eta^{5/2}\left[Z_0^+(\sqrt{\eta}) - Z_0^-(-\sqrt{\eta})\right] + 2\eta^2 + \eta + \frac{3}{2} ,$$

$$\eta = \eta_d \Omega , \qquad \eta_d = (\omega_A/\Omega_d)\left[1 - \frac{\alpha_c}{2q^2} - \frac{3\alpha_H G(0)}{4q^2}\right]^{-1} ,$$

and all other quantities are defined in Ref. 5.

The kinetic ballooning equation for the case of the slowing-down distribution is

$$\frac{d}{d\Theta}(1 + h^2)\frac{d\phi}{d\Theta} + \left\{\Omega\left(\Omega - \frac{\omega_p}{\omega_A}\right)\left(1 + h^2\right) + \left(\cos\Theta + h\sin\Theta\right) \times \left[\alpha_c + \frac{3}{4}\alpha_H G(\Theta)\right]\right\}\tilde{\phi}$$

$$= \frac{3\delta^2\alpha_H}{2f_0(\delta)\ln(1 + \delta^{-3})} \frac{(\cos\Theta + h\sin\Theta)G(\Theta)H(\eta,\delta)\tilde{\Phi}(\Theta = 2m\pi)}{1 - \frac{\alpha_c}{2q^2} - \frac{3\alpha_H G(0)}{4q^2}\left[1 - \frac{2\delta^2 H(\eta,\delta)}{f_0(\delta)\ln(1 + \delta^{-3})}\right]} , \tag{4}$$

where

$$\delta = \frac{v_c}{v_\alpha}, \quad v_\alpha = \sqrt{2E_\alpha/M_H}, \quad E_\alpha = 3.5 \text{ MeV},$$

$$f_0(\delta) = \frac{1}{\ln(1 + \delta^{-3})} \left\{1 + \frac{2}{3}\delta^2\left[\frac{1}{2}\ln\frac{(1+\delta)^2}{1 - \delta + \delta^2} - \sqrt{3}\left(\tan^{-1}\frac{2-\delta}{\sqrt{3}\delta} + \frac{\pi}{6}\right)\right]\right\},$$

$$\alpha_H = -\frac{Rq^2E_\alpha f_0(\delta)n_H'}{B^2/8\pi},$$

$$\eta_d = \left(\frac{2}{\varepsilon_p\alpha_c b_i}\right)^{1/2}\left(\frac{T_i}{\delta^2E_\alpha}\right)\left(\frac{Z_H}{Z_i}\right)\left[1 - \frac{\alpha_c}{2q^2} - \frac{3\alpha_H G(0)}{4q^2}\right]^{-1},$$

$$H(\eta,\delta) = \int_0^{\delta^{-1}} \frac{x^6\,dx}{(1 + x^3)(x^2 - \eta)},$$

with all other terms defined as in the case of the Maxwellian.

The notable differences between Eqs. (3) and (4) occur primarily in the resonant coupling terms. The velocity integral is now over a finite range (because of the cutoff at 3.5 MeV) and can no longer be expressed in terms of the plasma dispersion function. The $H(\eta,\delta)$ integral can, however, be evaluated analytically using a partial fractions decomposition; an outline of this procedure is given in Appendix A. The functions $\ln(1 + \delta^{-3})$ and $f_0(\delta)$ that appear in Eq. (4) are introduced from the normalization factor a_2 and the pressure moment of $f_{s.d.}$ [i.e., $p_{\perp H} = 1.5N_H(r)E_\alpha f_0(\delta)G(\Theta)$].

III. DISCUSSION OF RESULTS

In solving Eqs. (3) and (4) we have considered parameter ranges similar to those of Ref. 5. α_H/α_c has been varied over the range from 0 to 1/2; $b_i = k^2\rho_i^2/2 = 0.04$, and $q = 2$ [for Tokamak Fusion Test Reactor (TFTR)[7] parameters this implies a mode number of 14, assuming $r/a = 0.5$, $T_i = 10$ keV, and deuterium as the ion species]. R/r_p has been set at 6, where r_p is the background plasma scale length. This value has been chosen to account for alpha heating in the center of the plasma, which can lead to a steeper pressure gradient than would be given by setting R/r_p equal to the simple geometric aspect ratio (sensitivity of stability boundaries to R/r_p is examined in Fig. 4). Also, we have fixed b_0, the parameter that determines the width of the f_H distribution in pitch angle, at 10 (see Ref. 5). Again, the case of alphas in a deuterium plasma is considered here, implying that $Z_H/Z_i = 2$ and $M_H/M_i = 2$. The numerical solution procedure and the boundary conditions used in solving Eqs. (3) and (4) are the same as described in Ref. 5. The upper end Θ_{max} of the interval over which the ballooning equation is solved has been chosen as 3π here because this provides sufficient convergence. The only remaining parameters are T_i and T_e, the background ion and electron temperatures. T_e has been varied over the range from 10 keV to 40 keV, and we have taken $T_i = T_e$. T_e controls the effective temperature of the alpha slowing-down distribution through the critical velocity v_c (e.g., for $T_e = 20$ keV, $v_c/v_\alpha = 0.46$, where v_α is the birth velocity of the alphas); as T_e is raised, v_c/v_α increases, and the mean energy of the slowing-down distribution increases. However, due to the choice of $T_i = T_e$, the

location of the resonance between the precessional drift and the real frequency of the ballooning mode (which depends on ω_{*i} and thus on T_i) moves to higher energies with increasing T_e. The scaling of these two effects is such that increasing the background electron temperature is generally destabilizing even though it is increasing the mean energy of the hot species distribution.

An example of this dependence is shown in Fig. 1, where stability contours (at which $\omega_i/\omega_r = 0.05$) similar to those shown in Ref. 5 are plotted in the shear vs pressure gradient (s-α_c) parameter space. Here we choose $\alpha_H/\alpha_c = 0.3$ and vary T_e. Increasing T_e significantly enlarges the unstable region, and for $T_e = 40$ keV, the right portion of the stability boundary has moved off the figure to values of $\alpha_c > 1.8$. The widening of the unstable region in the lower left-hand side of the figure is in the range of shear and pressure gradient sampled by the central plasma regions in devices such as TFTR; such effects could thus become observable as either the alpha pressure or the background electron temperature is increased.

In Fig. 2, T_e is fixed at 20 keV and α_H/α_c is varied from 0 up to 0.5. This figure shows a trend similar to that in the analogous plot in Ref. 5 for the Maxwellian. That is, increasing α_H/α_c lowers the critical α_c on the left-hand side of the unstable region but shrinks the unstable region from the top and right-hand side. However, again because the central region of the tokamak (where the alpha population is peaked) is generally at low shear and low α_c, the lower left-hand side of the boundary (where the unstable region is enlarging) is the most relevant.

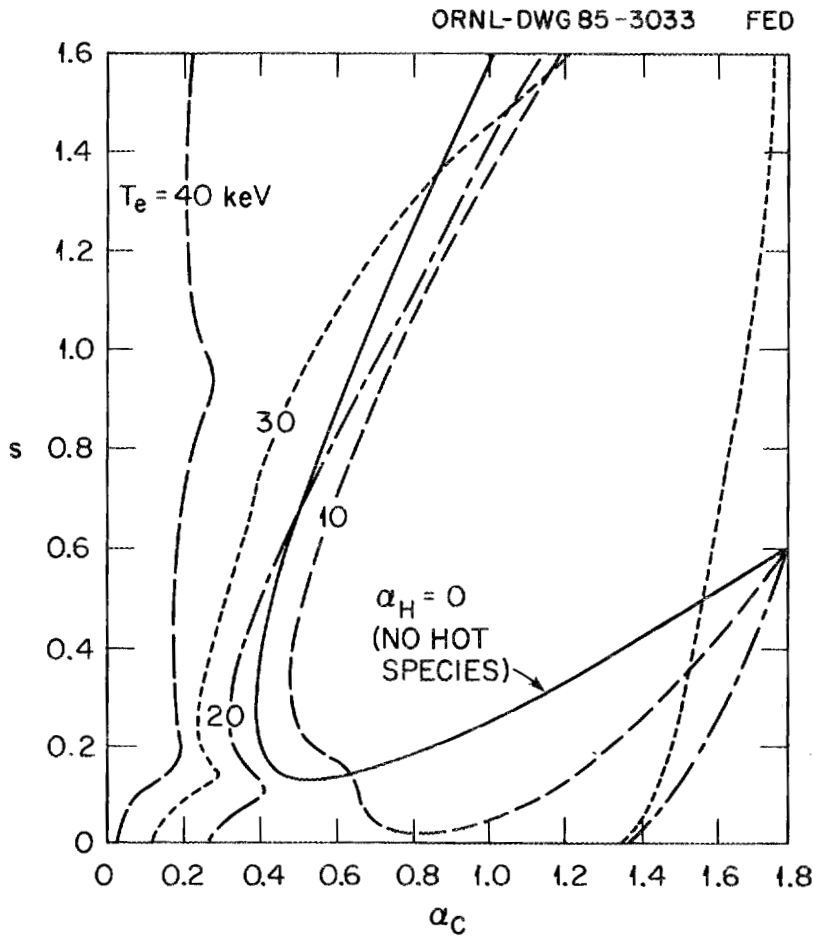

Fig. 1. Dependence of stability boundaries for slowing-down distribution on plasma electron temperature T_e (α_H/α_c = 0.3, q = 2, b_i = 0.04, T_e = 10, 20, 30, 40 keV).

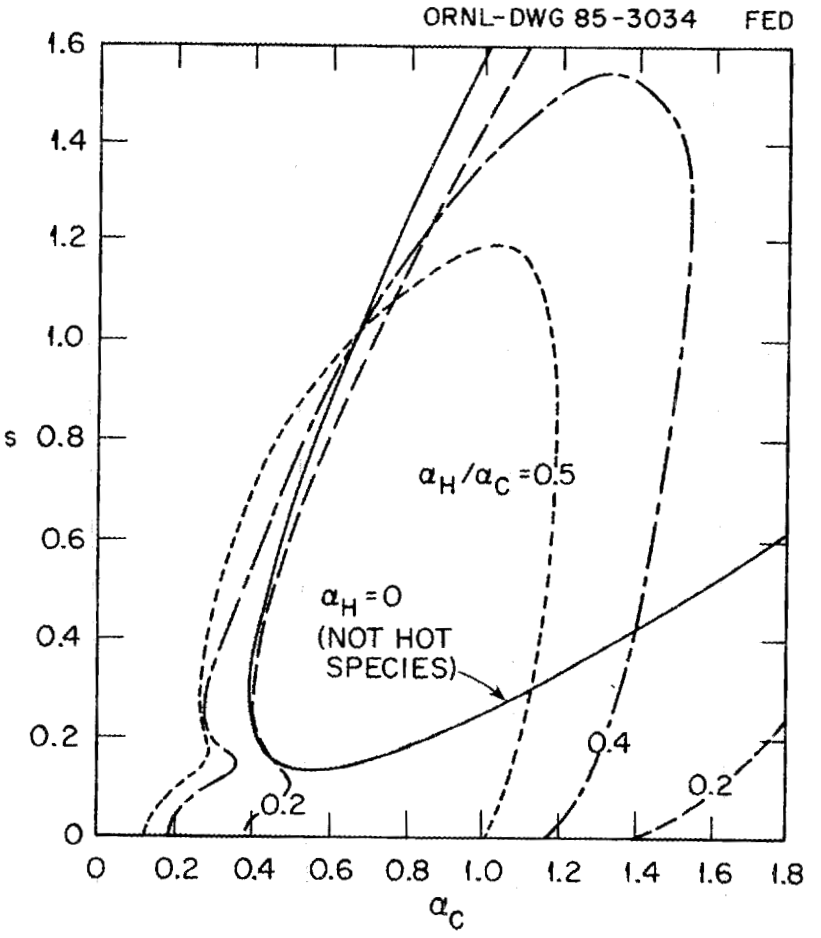

Fig. 2. Dependence of stability boundaries for slowing-down distribution on α_H/α_c with T_e = 20 keV, q = 2, b_i = 0.04.

For comparison, in Fig. 3 we plot the dependence of the stability boundaries on α_H/α_c for a Maxwellian with density and pressure moments equivalent to those of the slowing-down distribution of Fig. 2 with T_e = 20 keV (i.e., T_H/T_i = 49.1 from Table 1), keeping the other parameters the same as in Fig. 2. This indicates that the shrinkage of the unstable region at high values of α_H/α_c is greater for the slowing-down distribution than for the Maxwellian (i.e., α_H/α_c = 0.5 for the slowing-down model is about the same as α_H/α_c = 0.6 for the Maxwellian).

Figure 4 examines the sensitivity of stability boundaries to the background pressure gradient parameter R/r_p. Besides affecting the ballooning beta limit through the proportionality constant relating β_c and α_c (i.e., $\alpha_c = Rq^2\beta_c/r_p$), R/r_p also influences the degree of coupling between the hot and background species because ω_p/ω_{dH} scales as R/r_p. Thus, as R/r_p is lowered, the location of the resonance between the real frequency of the ballooning mode and the hot species drift frequency moves to lower energies, causing the $H(\eta,\delta)$ integral to be smaller and lowering the extent of hot-background coupling. This characteristic can be seen in Fig. 4, where cases with T_e = 30 keV, q = 2, α_H/α_c = 0.3, b_i = 0.04, and R/r_p = 10, 8, 6, and 4 are given. For the R/r_p = 10 and 8 cases, the right-hand boundary to the most unstable root present has moved off the right-hand side of the figure.

Next we compare the growth rates and critical betas obtained using the slowing-down distribution with those resulting from the Maxwellian. To put the comparisons on an equal footing, a basis must be determined for choosing T_H, the temperature of the Maxwellian, and the relation between the somewhat differently defined α_H parameters for the two

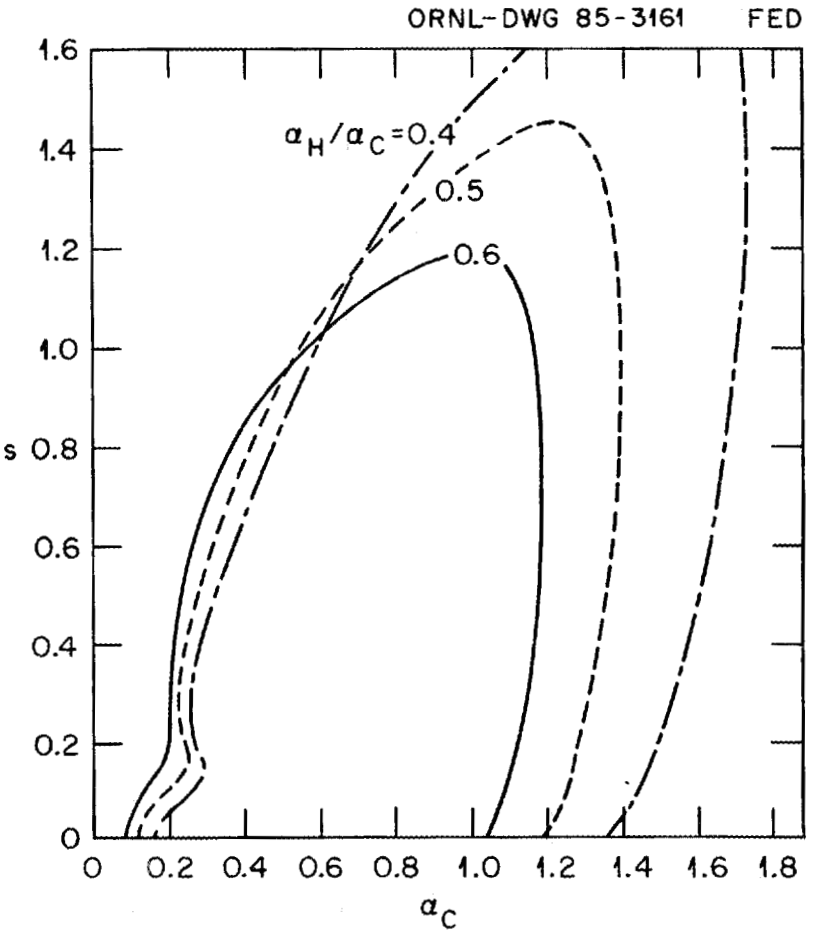

Fig. 3. Dependence of stability boundaries for Maxwellian distribution on α_H/α_c with T_H/T_i = 49.1, q = 2, b_i = 0.04.

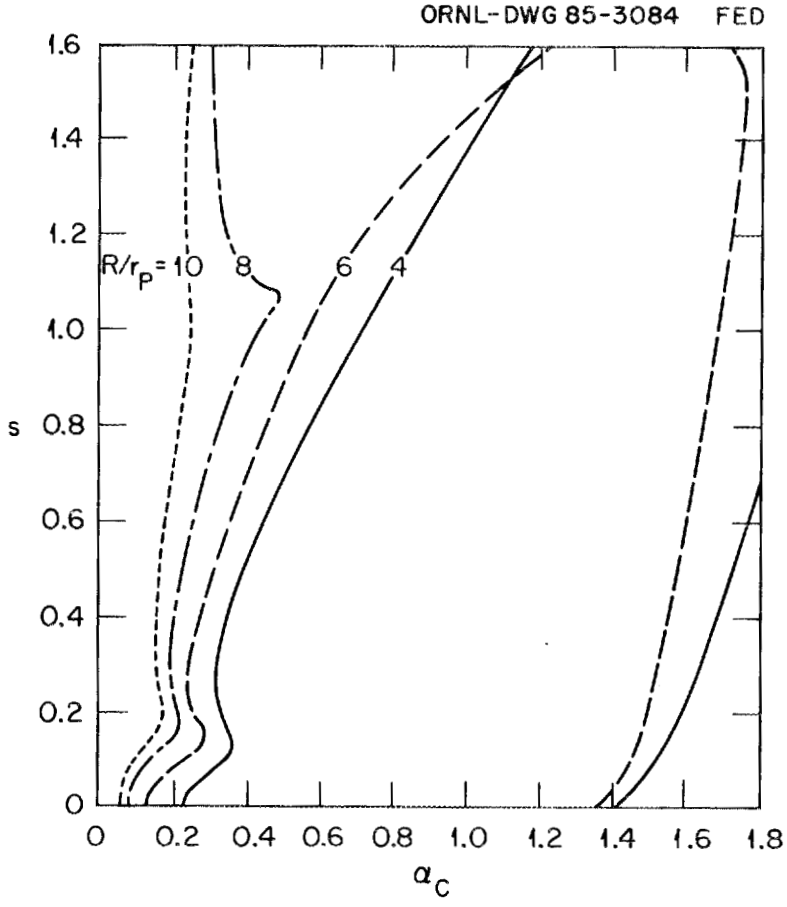

Fig. 4. Dependence of stability boundaries for slowing-down distribution on R/r_p with T_e = 30 keV, α_H/α_c = 0.3, q = 2, and b_i = 0.04.

models [α_H is defined following Eqs. (3) and (4)]. We choose to compare distributions with equal density and pressure moments. This implies that $\alpha_{H,Max} = \alpha_{H,s.d.}$ and

$$T_H = E_\alpha f_0(\delta) \ . \tag{5}$$

Table 1 indicates values of T_H/T_i (taking $T_e = T_i$), δ, and T_e that satisfy our criterion.

Table 1.

T_e (keV)	δ (= v_c/v_α)	T_H/T_i
10	0.33	83.7
20	0.46	49.1
30	0.56	35.6
40	0.65	28.2

These parameters are used in the following plots, which compare results from the two distributions.

In Fig. 5 the growth rate vs α_H is examined at fixed values of s and α_c ($s = 0.6$, $\alpha_c = 0.8$) for T_e = 10, 20, 30, and 40 keV for the slowing-down distribution and at the values of T_H/T_i given in the table for the Maxwellian. The Maxwellian distribution growth rates are somewhat higher for the T_e = 10-, 20-, and 30-keV cases, and the slowing-down distribution growth rates are higher for the T_e = 40-keV case.

In Fig. 6 we consider the effect of the two distributions on the left-hand stability boundary (of Figs. 1 and 2) at a fixed value of s

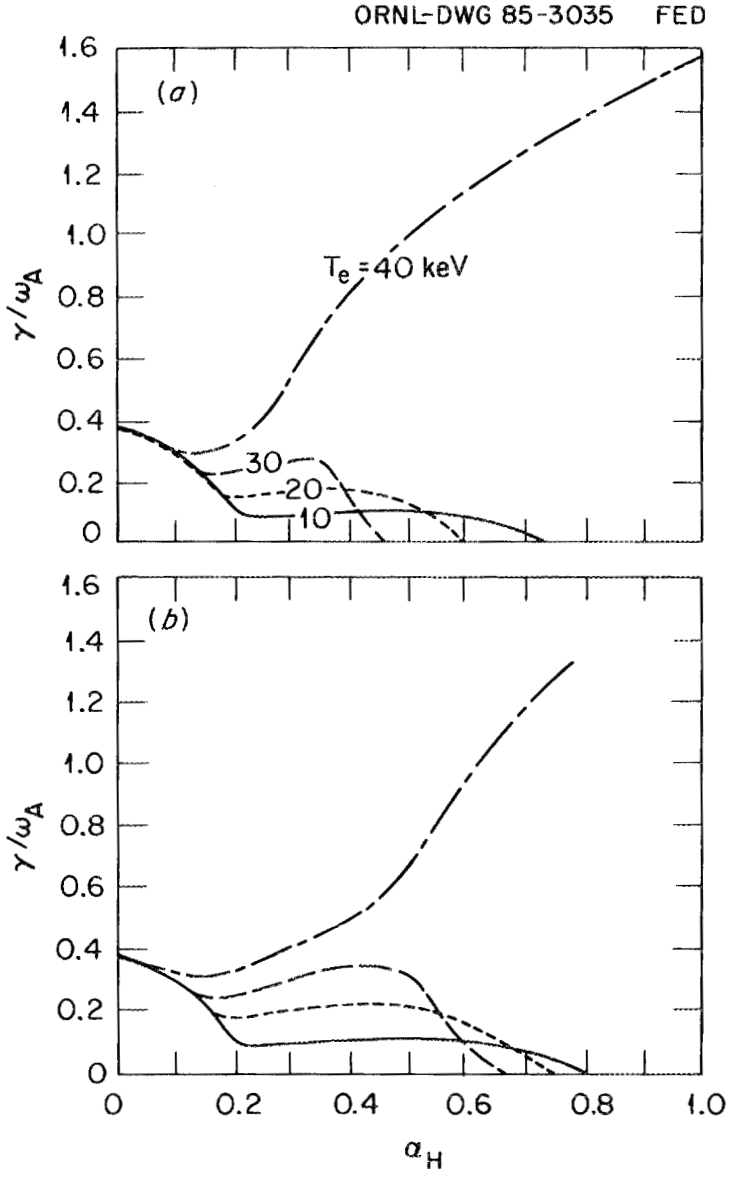

Fig. 5. Growth rate vs α_H at s = 0.6, α_c = 0.8 for the slowing-down (upper plot) and Maxwellian distribution (lower plot) function models for T_e = 10, 20, 30, 40 keV in the case of the slowing-down model and using values of T_H/T_i from Table 1 in the case of the Maxwellian (T_H/T_i = 83.7 – solid line, T_H/T_i = 49.1 – short-dashed line, T_H/T_i = 35.6 – long-dashed line, T_H/T_i = 28.2 – short- and long-dashed line).

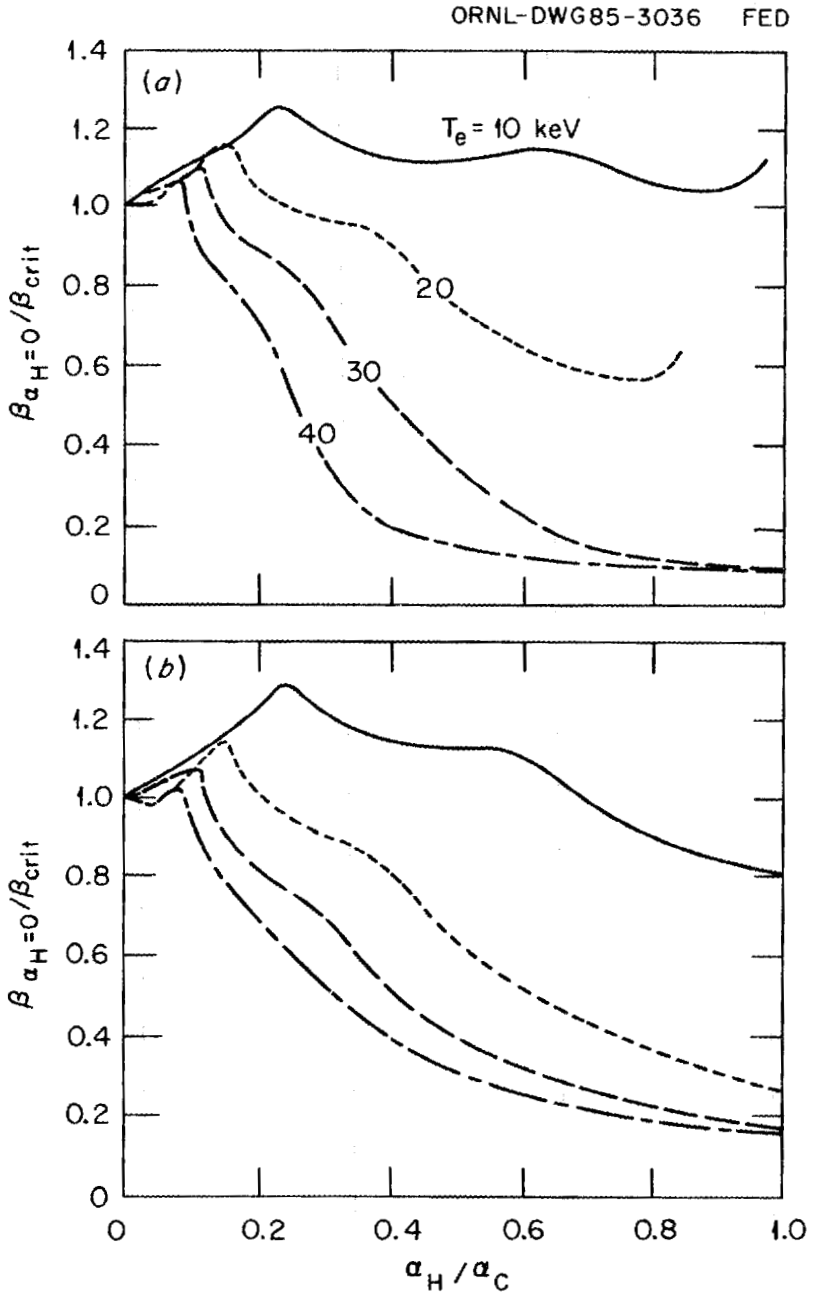

Fig. 6. Ratio of critical beta for ballooning instability with alphas to that without alphas vs α_H/α_c for the slowing-down (upper plot) and Maxwellian distribution function (lower plot) models at s = 0.6 with T_e = 10, 20, 30, and 40 keV for the slowing-down model and with T_H/T_i from Table 1 in the case of the Maxwellian (using same legend as Fig. 5).

($s = 0.6$) as a function of α_H/α_c. Because α_c is proportional to the beta of the thermal plasma ($\beta = \varepsilon_p\alpha_c/q^2$), we have expressed the vertical axis in terms of the critical plasma beta for the onset of ballooning (i.e., $\omega_i/\omega_r > 0.05$ here), normalized to the critical value if no hot species were present ($\beta_{\alpha_H=0}$). These curves again show similar dependences but a somewhat more rapid falloff of the beta limit for the slowing-down distribution, especially with $T_e = 30$ and 40 keV. An interesting feature of these curves is the slight stabilization ($\beta_{crit}/\beta_{\alpha_H=0} > 1$) that is present at the lower values of α_H/α_c ($\lesssim 0.2$). However, at the more typical values of α_H/α_c (1/3 to 1/2), the background beta limit drops more than fivefold from its value without alphas.

A further consideration in assessing the effect of alphas on tokamak stability is the dependence of the growth rate on the radial location within the plasma. To examine this, we have parameterized quantities in terms of shear, which typically varies from 0 to 4 in going from the magnetic axis to the outside edge of the plasma. A self-consistent equilibrium code has been employed to calculate the dependence of q and α_c on s as one goes from the central region to the outside. This information is then used in the stability calculation. For the case considered here the equilibrium code was run with $R/a = 3.4$ and $\langle\beta\rangle = 3\%$. The ratio α_H/α_c was fixed at 0.3 over the whole cross section and T_e was set at 20 keV. More realistically, one might want to allow radial variation in these quantities as well, but this level of detailed modeling has not been pursued yet. In Fig. 7 we plot growth rates as a function of shear (i.e., radial location) for the cases with no alphas present and with alphas for the Maxwellian and

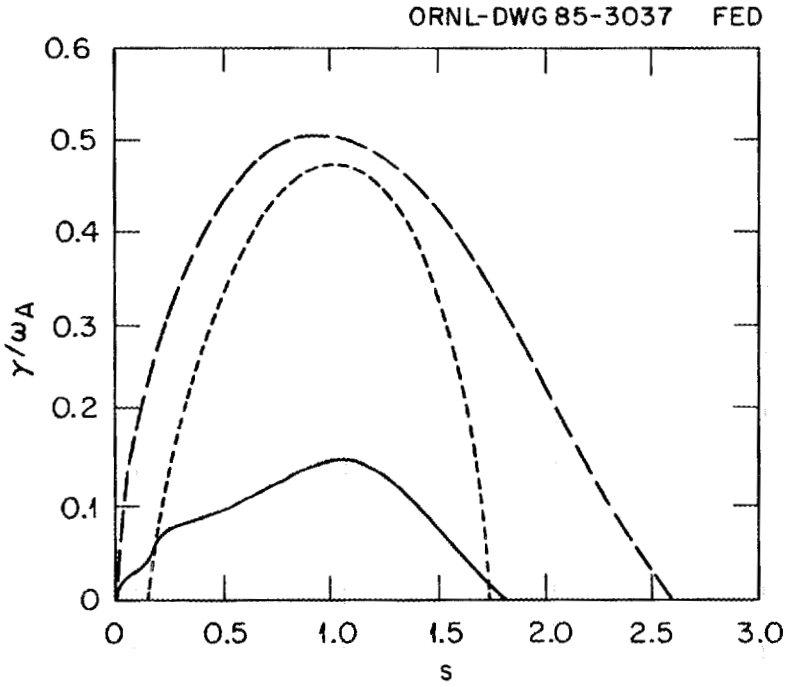

Fig. 7. Dependence of growth rate on shear along an equilibrium trajectory going from center of plasma to outer flux surfaces for $\alpha_H/\alpha_c = 0.3$, $T_e = 20$ keV ($T_H/T_i = 49.1$ in the case of the Maxwellian) for three cases: no alphas present (short-dashed line), a Maxwellian distribution of alphas (solid line), and a slowing-down distribution of alphas (long-dashed line).

slowing-down distribution function models. The slowing-down model results in the highest growth rates and destabilizes a larger portion of the cross section. Both the Maxwellian and the slowing-down distributions result in finite growth rates further into the central region of the plasma than is the case in the absence of alphas.

IV. CONCLUSIONS

We have found that an alpha slowing-down distribution results in a stronger influence on the stability of ballooning modes than the Maxwellian model for distributions with equal density and pressure moments. As indicated in the preceding figures, this appears in the following areas. First, the unstable region for ballooning is enlarged to small values of shear and pressure gradient as both α_H/α_c and T_e are increased; such regimes will characterize the central regions of tokamak breakeven devices such as TFTR and could be observable for the projected ranges of alpha pressure and plasma temperature. Also, at high values of α_H/α_c (0.3 to 0.5), the slowing-down model leads to a closing-off of the unstable region at high shear and a shrinkage in its size with a somewhat lower fraction of alphas than would be required with the Maxwellian. In such regimes (high shear and α_H/α_c) the alpha component can have a favorable influence on ballooning stability. Next, examining the growth rate and critical beta at a fixed value of shear ($s = 0.6$) indicated that the slowing-down distribution resulted in higher growth rates and lower beta limits than the Maxwellian for background temperatures appropriate to the central regions of such devices. Finally, following the radial variation of the growth rate from the center to the outside of a tokamak equilibrium demonstrated

that the slowing-down model growth rates were significantly higher and remained finite over a larger fraction of the plasma cross section than either the Maxwellian model or the case with no alphas present.

In addition, a new feature of the slowing-down distribution model is the sensitivity to the background plasma electron temperature. Based on the previous Maxwellian results,[5] one might have expected that increasing T_e (which increases the mean energy of the slowing-down distribution) would provide increased decoupling between hot and background species and thus increased stability. However, due to the increase in the real frequency of the ballooning mode with T_e (where we chose $T_i = T_e$), the interaction with the trapped-particle precessional frequency tracks with the increasing mean alpha energy, resulting in increasing destabilization as T_e is raised.

REFERENCES

[1]P. J. Catto, R. J. Hastie, and J. W. Connor, Plasma Phys. Controlled Fusion 27, 307 (1985).

[2]J. W. Connor, R. J. Hastie, T. J. Martin, and M. F. Turner, in Proceedings of the Third Joint Varenna-Grenoble International Symposium on Heating in Toroidal Plasmas (Commission of the European Communities, Brussels, 1982), Vol. 1, p. 65; R. J. Hastie and K. W. Hesketh, Nucl. Fusion 21, 651 (1981).

[3]M. N. Rosenbluth, S. T. Tsai, J. W. Van Dam, and M. G. Engquist, Phys. Rev. Lett. 51, 1967 (1983).

[4]J. Weiland and L. Chen, Phys. Fluids 28, 1359 (1985).

[5]D. A. Spong, D. J. Sigmar, W. A. Cooper, and D. E. Hastings, Phys. Fluids 28, 2494 (1985).

[6]G. Rewoldt and W. M. Tang, Nucl. Fusion 24, 1573 (1984).

[7]P. C. Efthimon, M. Bell, W. R. Blanchard, N. Bretz, J. L. Cecchi, J. Coonrod, S. Davis, H. F. Dylla, R. Fonck, and H. P. Furth, Phys. Rev. Lett. 52, 1492 (1984).

APPENDIX A: EVALUATION OF THE $H(\eta,\delta)$ INTEGRAL

The first step in performing the $H(\eta,\delta)$ integral is a partial fractions decomposition of the integrand:

$$\frac{x^6}{(1+x^3)(x^2-\eta)} = x - \frac{1}{3(\eta-1)(x+1)} + \left(\frac{\eta^3}{\eta^3-1}\right)\frac{\eta x-1}{x^2-\eta}$$
$$+ \frac{1}{3(\eta^2+\eta+1)}\left[\left(\frac{\eta-1}{2}\right)\frac{2x-1}{x^2-x+1} - \frac{3}{2}\left(\eta+1\right)\frac{x+1}{x^3+1}\right] . \tag{A.1}$$

Integrating this from 0 to t_1 ($t_1 = \delta^{-1}$) then yields the following:

$$H(\eta,\delta) = \frac{t_1^2}{2} - \frac{\ln(t_1+1)}{3(\eta-1)} + \frac{\eta^3}{\eta^3-1}\left\{\frac{\eta}{2}\left[\log(t_1-\eta) - \log(-\eta)\right]\right.$$
$$\left. - \frac{1}{2\sqrt{\eta}}\left[\log(t_1-\sqrt{\eta}) - \log(-\sqrt{\eta}) - \log(t_1+\sqrt{\eta}) + \log(\sqrt{\eta})\right]\right\}$$
$$+ \frac{1}{3(\eta^2+\eta+1)}\left[\frac{\eta-1}{2}\ln(t_1^2-t_1+1)\right.$$
$$- \sqrt{3}(\eta+1)\tan^{-1}\frac{\sqrt{3}}{3}(2t_1-1)$$
$$\left. - \sqrt{3}(\eta+1)\tan^{-1}\left(\frac{1}{\sqrt{3}}\right)\right] . \tag{A.2}$$

In performing these integrations, we have assumed that $|\eta| \leq t_1^2$. Also, for clarity we have denoted all of the logarithm functions in Eq. (A.2)

that have complex arguments as "log" and all of those with real arguments as "ln."

The log terms arise from the third term [proportional to $(x^2 - \eta)^{-1}$] of Eq. (A.1). To demonstrate that this form properly treats the residue at $x = \pm\sqrt{\eta}$, we consider a contour integral that encloses the pole for the first part of the third term in Eq. (A.1) (similar arguments apply to the second part). Our contour consists of the path along the real axis from $z = 0$ to $z = t_1$, followed by the quarter-circle from $z = t_1$ to $z = it_1$ (i.e., $z = t_1 e^{i\theta}$, $0 \leq \theta \leq \pi/2$) and followed by the path along the imaginary axis from $z = it_1$ to $z = 0$. The integral we consider is

$$I = \oint \frac{z\,dz}{z^2 - \eta} = I_1 + I_2 + I_3 \,. \tag{A.3}$$

Because the contour encloses the pole at $z = \sqrt{\eta}, i$ $I = \pi i$. The individual parts of I are then

$$I_1 = \int_0^{t_1} \frac{z\,dz}{z^2 - \eta} = \frac{1}{2}\log(z^2 - \eta)\Big|_0^{t_1} = \frac{1}{2}\Big[\underset{(4th)}{\log(t_1^2 - \eta)} - \underset{(3rd)}{\log(-\eta)}\Big]$$

$$I_2 = \int_{t_1}^{it_1} \frac{z\,dz}{z^2 - \eta} = \frac{1}{2}\log(z^2 - \eta)\Big|_{t_1}^{it_1} = \frac{1}{2}\Big[\underset{(3rd)}{\log(-t_1^2 - \eta)} - \underset{(4th)}{\log(t_1^2 - \eta)}\Big]$$

$$+ \pi i$$

$$I_3 = \int_{it_1}^{0} \frac{z\,dz}{z^2 - \eta} = \frac{1}{2}\log(z^2 - \eta)\Big|_{it_1}^{0} = \frac{1}{2}\Big[\underset{(3rd)}{\log(-\eta)} - \underset{(3rd)}{\log(-t_1^2 - \eta)}\Big] \,,$$

with I_1 being the integral that enters into Eq. (A.2). Under each term we have noted the quadrant in which the argument of the log function is

located, assuming that η is in the first quadrant and that $|\eta| < t_1^2$. I_2 picks up a term πi because in going from the lower limit to the upper limit of this integral, the argument of the log function has gone from the fourth to the third quadrant, thus passing in the counterclockwise sense over the branch cut for the log function along the negative real axis. It is clear then that the sum of the three integrals equals πi, with the integral along the quarter-circle (I_2) contributing this term.

This calculation demonstrates that the $H(\eta,\delta)$ integral is somewhat different in nature from that resulting when a Maxwellian is used (involving the plasma dispersion function). Closing the contour in the upper half-plane results in a finite contribution from the upper half of the contour. This arises from the finite cutoff velocity, which is necessary with the slowing-down distribution to obtain a convergent integral.

ORNL/TM-9688
Dist. Category UC-20 g

INTERNAL DISTRIBUTION

1. W. E. Bryan
2. B. A. Carreras
3-4. W. A. Cooper
5. J. Sheffield
6-7. D. J. Sigmar
8-12. D. A. Spong
13-14. Laboratory Records Department
15. Laboratory Records, ORNL-RC
16. Document Reference Section
17. Central Research Library
18. Fusion Energy Division Library
19-20. Fusion Energy Division Publications Office
21. ORNL Patent Office

EXTERNAL DISTRIBUTION

22-23. D. E. Hastings, Massachusetts Institute of Technology, 77 Massachusetts Avenue, Cambridge, MA 02139
24. Office of the Assistant Manager for Energy Research and Development, Department of Energy, Oak Ridge Operations Office, P. O. Box E, Oak Ridge, TN 37831
25. J. D. Callen, Department of Nuclear Engineering, University of Wisconsin, Madison, WI 53706
26. J. F. Clarke, Office of Fusion Energy, Office of Energy Research, ER-50, Germantown, U.S. Department of Energy, Washington, DC 20545

27. R. W. Conn, Department of Chemical, Nuclear, and Thermal Engineering, University of California, Los Angeles, CA 90024
28. S. O. Dean, Director, Fusion Energy Development, Science Applications International Corporation, 2 Professional Drive, Suite 249, Gaithersburg, MD 20879
29. H. K. Forsen, Bechtel Group, Inc., Research Engineering, P. O. Box 3965, San Francisco, CA 94105
30. J. R. Gilleland, GA Technologies, Inc., Fusion and Advanced Technology, P.O. Box 81608, San Diego, CA 92138
31. R. W. Gould, Department of Applied Physics, California Institute of Technology, Pasadena, CA 91125
32. R. A. Gross, Plasma Research Library, Columbia University, New York, NY 10027
33. D. M. Meade, Princeton Plasma Physics Laboratory, P.O. Box 451, Princeton, NJ 08544
34. M. Roberts, International Programs, Office of Fusion Energy, Office of Energy Research, ER-52, U.S. Department of Energy, Washington, DC 20545
35. W. M. Stacey, School of Nuclear Engineering, Georgia Institute of Technology, Atlanta, GA 30332
36. D. Steiner, Nuclear Engineering Department, NES Building, Tibbetts Avenue, Rensselaer Polytechnic Institute, Troy, NY 12181
37. R. Varma, Physical Research Laboratory, Navrangpura, Ahmedabad 380009, India
38. Bibliothek, Max-Planck Institut fur Plasmaphysik, D-8046 Garching, Federal Republic of Germany
39. Bibliothek, Institut fur Plasmaphysik, KFA, Postfach 1913, D-5170 Julich, Federal Republic of Germany
40. Bibliotheque, Centre des Recherches en Physique des Plasmas, 21 Avenue des Bains, 1007 Lausanne, Switzerland
41. Bibliotheque, Service du Confinement des Plasmas, CEA, B.P. No. 6, 92 Fontenay-aux-Roses (Seine), France
42. Documentation S.I.G.N., Departement de la Physique du Plasma et de la Fusion Controlee, Centre d'Etudes Nucleaires, B.P. 85, Centre du Tri, 38041 Cedex, Grenoble, France

43. Library, Culham Laboratory, UKAEA, Abingdon, Oxfordshire, OX14 3DB, England
44. Library, FOM-Instituut voor Plasma-Fysica, Rijnhuizen, Edisonbaan 14, 3439 MN Nieuwegein, The Netherlands
45. Library, Institute of Plasma Physics, Nagoya University, Nagoya 464, Japan
46. Library, International Centre for Theoretical Physics, Trieste, Italy
47. Library, Laboratorio Gas Ionizatti, CP 56, I-00044 Frascati, Rome, Italy
48. Library, Plasma Physics Laboratory, Kyoto University, Gokasho, Uji, Kyoto, Japan
49. Plasma Research Laboratory, Australian National University, P.O. Box 4, Canberra, A.C.T. 2000, Australia
50. Thermonuclear Library, Japan Atomic Energy Research Institute, Tokai-mura, Ibaraki Prefecture, Japan
51. G. A. Eliseev, I. V. Kurchatov Institute of Atomic Energy, P. O. Box 3402, 123182 Moscow, U.S.S.R.
52. V. A. Glukhikh, Scientific-Research Institute of Electro-Physical Apparatus, 188631 Leningrad, U.S.S.R.
53. I. Shpigel, Institute of General Physics, U.S.S.R. Academy of Sciences, Ulitsa Vavilova 38, Moscow, U.S.S.R.
54. D. D. Ryutov, Institute of Nuclear Physics, Siberian Branch of the Academy of Sciences of the U.S.S.R., Sovetskaya St. 5, 630090 Novosibirsk, U.S.S.R.
55. V. T. Tolok, Kharkov Physical-Technical Institute, Academical St. 1, 310108 Kharkov, U.S.S.R.
56. Library, Institute of Physics, Academia Sinica, Beijing, Peoples Republic of China
57. N. A. Davies, Office of the Associate Director, Office of Fusion Energy, Office of Energy Research, ER-51, Germantown, U.S. Department of Energy, Washington, DC 20545
58. D. B. Nelson, Director, Division of Applied Plasma Physics, Office of Fusion Energy, Office of Energy Research, ER-54, Germantown, U.S. Department of Energy, Washington, DC 20545

59. E. Oktay, Division of Confinement Systems, Office of Fusion Energy, Office of Energy Research, ER-55, Germantown, U.S. Department of Energy, Washington, DC 20545
60. A. L. Opdenaker, Fusion Systems Design Branch, Division of Development and Technology, Office of Fusion Energy, Office of Energy Research, ER-532, Germantown, U.S. Department of Energy, Washington, DC 20545
61. W. Sadowski, Fusion Theory and Computer Services Branch, Division of Applied Plasma Physics, Office of Fusion Energy, Office of Energy Research, ER-541, Germantown, U.S. Department of Energy, Washington, DC 20545
62. P. M. Stone, Fusion Systems Design Branch, Division of Development and Technology, Office of Fusion Energy, Office of Energy Research, ER-532, Germantown, U.S. Department of Energy, Washington, DC 20545
63. J. M. Turner, International Programs, Office of Fusion Energy, Office of Energy Research, ER-52, Germantown, U.S. Department of Energy, Washington, DC 20545
64. R. E. Mickens, Atlanta University, Department of Physics, Atlanta, GA 30314
65. M. N. Rosenbluth, RLM 11.218, Institute for Fusion Studies, University of Texas, Austin, TX 78712
66. Theory Department Read File, c/o D. W. Ross, Institute for Fusion Studies, University of Texas, Austin, TX 78712
67. Theory Department Read File, c/o R. C. Davidson, Director, Plasma Fusion Center, NW 16-202, Massachusetts Institute of Technology, Cambridge, MA 02139
68. Theory Department Read File, c/o F. W. Perkins, Princeton Plasma Physics Laboratory, P.O. Box 451, Princeton, NJ 08544
69. Theory Department Read File, c/o L. Kovrizhnykh, Lebedev Institute of Physics, Academy of Sciences, 53 Leninsky Prospect, 117924 Moscow, U.S.S.R.
70. Theory Department Read File, c/o B. B. Kadomtsev, I. V. Kurchatov Institute of Atomic Energy, P.O. Box 3402, 123182 Moscow, U.S.S.R.

71. Theory Department Read File, c/o T. Kamimura, Institute of Plasma Physics, Nagoya University, Nagoya 464, Japan
72. Theory Department Read File, c/o C. Mercier, Euratom-CEA, Service des Recherches sur la Fusion Controlee, Fontenay-aux-Roses (Seine), France
73. Theory Department Read File, c/o T. E. Stringer, JET Joint Undertaking, Culham Laboratory, Abingdon, Oxfordshire OX14 3DB, England
74. Theory Department Read File, c/o K. Roberts, Culham Laboratory, Abingdon, Oxfordshire OX14 3DB, England
75. Theory Department Read File, c/o D. Biskamp, Max-Planck-Institut fur Plasmaphysik, D-8046 Garching, Federal Republic of Germany
76. Theory Department Read File, c/o T. Takeda, Japan Atomic Energy Research Institute, Tokai-mura, Ibaraki Prefecture, Japan
77. Theory Department Read File, c/o C. S. Liu, GA Technologies, Inc., P.O. Box 81608, San Diego, CA 92138
78. Theory Department Read File, c/o L. D. Pearlstein, L-630, Lawrence Livermore National Laboratory, P.O. Box 5511, Livermore, CA 94550
79. Theory Department Read File, c/o R. Gerwin, CTR Division, Los Alamos National Laboratory, P.O. Box 1663, Los Alamos, NM 87545
80. G. Swanson, Auburn University, Auburn, AL 36849
81. H. L. Berk, Institute for Fusion Studies, University of Texas, Austin, TX 78712
82. H. Biglari, Princeton Plasma Physics Laboratory, P.O. Box 451, Princeton, NJ 08544
83. P. J. Catto, Science Applications International Corporation, 934 Pearl Street, Boulder, CO 80302
84. L. Chen, Princeton Plasma Physics Laboratory, P.O. Box 451, Princeton, NJ 08544
85. N. Dominguez, Institute for Fusion Studies, University of Texas, Austin, TX 78712
86. J. Freidberg, Massachusetts Institute of Technology, 77 Massachusetts Avenue, Cambridge, MA 02139

87. J. Gaffey, IPST, University of Maryland, College Park, MD 20742
88. T. S. Hahm, Institute for Fusion Studies, University of Texas, Austin, TX 78712
89. T. Ramos, 26-277, Massachusetts Institute of Technology, 77 Massachusetts Avenue, Cambridge, MA 02139
90. G. Rewoldt, Princeton Plasma Physics Laboratory, P.O. Box 451, Princeton, NJ 08544
91. M. Rosenberg, JAYCOR, P.O. Box 85154, San Diego, CA 92138
92. D. P. Stotler, Institute for Fusion Studies, University of Texas, Austin, TX 78712
93. B. Tang, Princeton Plasma Physics Laboratory, P.O. Box 451, Princeton, NJ 08544
94. K. T. Tsang, Science Applications International Corporation, 934 Pearl Street, Boulder, CO 80302
95. J. W. Van Dam, Institute for Fusion Studies, University of Texas, Austin, TX 78712
96. S. Zweben, Princeton Plasma Physics Laboratory, P.O. Box 451, Princeton, NJ 08544

97-252. Given distribution as shown in TIC-4500, Magnetic Fusion Energy (Category Distribution UC-20 g: Theoretical Plasma Physics)